



Holocene Temperature Variations in Semi-Arid Central Mongolia—A Chronological and Sedimentological Perspective From a 7400-year Lake Sediment Record From the Khangai Mountains

OPEN ACCESS

Edited by:

Nadia Solovieva,
University College London,
United Kingdom

Reviewed by:

Henry Lamb,
Aberystwyth University,
United Kingdom
Larisa B. Nazarova,
Alfred Wegener Institute Helmholtz
Centre for Polar and Marine Research
(AWI), Germany

*Correspondence:

Marcel Bliedtner
marcel.bliedtner@uni-jena.de

Specialty section:

This article was submitted to
Quaternary Science, Geomorphology
and Paleoenvironment,
a section of the journal
Frontiers in Earth Science

Received: 01 April 2022

Accepted: 28 April 2022

Published: 12 May 2022

Citation:

Bliedtner M, Strobel P, Struck J,
Salazar G, Szidat S, Nowaczyk N,
Bazarradnaa E, Lloren R, Dubois N,
Haberzettl T and Zech R (2022)
Holocene Temperature Variations in
Semi-Arid Central Mongolia—A
Chronological and Sedimentological
Perspective From a 7400-year Lake
Sediment Record From the
Khangai Mountains.
Front. Earth Sci. 10:910782.
doi: 10.3389/feart.2022.910782

Marcel Bliedtner^{1*}, Paul Strobel¹, Julian Struck¹, Gary Salazar², Sönke Szidat², Norbert Nowaczyk³, Enkhtuya Bazarradnaa⁴, Ronald Lloren^{5,6}, Nathalie Dubois^{5,6}, Torsten Haberzettl⁷ and Roland Zech¹

¹Institute of Geography, Friedrich Schiller University Jena, Jena, Germany, ²Department of Chemistry, Biochemistry and Pharmaceutical Sciences and Oeschger Centre for Climate Change Research, University of Bern, Bern, Switzerland, ³Section Climate Dynamics and Landscape Evolution, GFZ German Research Centre for Geosciences, Potsdam, Germany, ⁴Institute of Plant and Agricultural Sciences, Mongolian University of Life Sciences, Darkhan, Mongolia, ⁵Department of Surface Waters Research and Management, Eawag, Dübendorf, Switzerland, ⁶Department of Earth Sciences, ETH Zürich, Zürich, Switzerland, ⁷Physical Geography, Institute for Geography and Geology, University of Greifswald, Greifswald, Germany

Semi-arid Mongolia is a highly sensitive region to climate changes, but the region's Holocene paleoclimatic evolution and its underlying forcing mechanisms have been the subject of much recent debate. Here we present a continuous 7.4 ka sediment record from the high-altitude Shireet Naiman Nuur (Nuur = lake) in the central Mongolian Khangai Mountains. We extensively dated the sediments and analyzed elemental composition and bulk isotopes for lake sediment characterization. Our results show that ¹⁴C-dating of bulk organic carbon and terrestrial macrofossils provide a robust and precise chronology for the past 7.4 ± 0.3 cal ka BP at Shireet Naiman Nuur and ¹⁴C-ages are mostly in stratigraphic order. The ¹⁴C-based chronology is confirmed by paleomagnetic secular variations, which resemble the predictions of spherical harmonic geomagnetic field models. The very good chronological control makes paleomagnetic secular variation stratigraphy a powerful tool for evaluating and refining regional ¹⁴C-chronologies when compared to the record presented here. The lake sediment proxies TOC, N, log (Ca/Ti) and log (Si/Ti) reveal increased lake primary productivity and high growing season temperatures from 7.4 ± 0.3 to 4.3 ± 0.2 cal ka BP, which is likely the result of stronger summer insolation and pronounced warming. Reduced summer insolation thereafter results in decreased productivity and low growing season temperatures at Shireet Naiman Nuur from 4.3 ± 0.3 cal ka BP until present day. The globally acknowledged 4.2 ka event also appears as a pronounced cooling event at Shireet Naiman Nuur, and additional abrupt cooling events occurred during minima in total solar irradiance at ~3.4, 2.8 and 2.4 ka BP. Low lake primary productivity and growing season temperatures are likely the result of longer ice cover periods at the high-altitude (2,429 m a.s.l.) Shireet Naiman Nuur. This leads to

shorter mixing periods of the lake water which is supported by more positive $\delta^{13}\text{C}_{\text{TOC}}$ because of increased incorporation of dissolved HCO_3^- by aquatic producers during periods of longer ice cover.

Keywords: semi-arid Mongolia, lake sediments, radiocarbon dating, paleomagnetic secular variations, paleoenvironmental changes

INTRODUCTION

Humans have become a major factor controlling landscape and environmental changes during the (Paleo) Anthropocene, which is reflected in increased soil erosion, global climate warming and extreme pressure on natural resources (Crutzen, 2002). This holds especially true for semi-arid regions, such as Mongolia, where rising temperatures and increased drought conditions are anticipated for the upcoming decades (Dai, 2011; IPCC, 2021). Mongolia is a highly sensitive region to climate changes due to its continentality and complex climate forcing characterized by the interplay of several large-scale atmospheric circulation patterns affecting moisture advection and precipitation variability (D'Arrigo et al., 2000; Aizen et al., 2001). The cold and dry winter climate is controlled by the Siberian High while moisture is supplied during summer months by the mid-latitude Westerlies and the low-latitude East Asian Summer Monsoon (EASM) (Hoerling et al., 2001; Mohtadi et al., 2016). So far, only little is known about the Holocene climate variability and its forcing mechanisms in semi-arid Mongolia. Besides climate changes, the semi-arid Mongolian steppe regions are also highly affected by anthropogenic land use and landscape modification, which is mostly reflected in vegetation clearance, overgrazing and soil erosion (Brugger et al., 2018; Huang et al., 2018; Unkelbach et al., 2021). The long history of mobile pastoral economies, the rise of nomadic empires, and the post-communism herding expansion strongly influenced landscape changes and modified landscape during the past (Fernández-Giménez et al., 2017). However, when and to which degree humans have affected the Mongolian steppe ecosystems is poorly understood. Moreover, it remains especially difficult to disentangle anthropogenic from natural paleoclimatic causes for vegetation and landscape changes.

So far, paleoenvironmental information for the semi-arid Mongolian steppe regions has been mostly derived from lake sediments and pollen-based reconstructions. For central Mongolia, these studies indicate more arid conditions during the Middle Holocene by increased Chenopodiaceae pollen scores and more humid conditions thereafter (Fowell et al., 2003; Prokopenko et al., 2007; Wang et al., 2011). However, human influence since ~4 ka might bias pollen reconstructions during the Late Holocene (Fowell et al., 2003; Brugger et al., 2018; Unkelbach et al., 2021). Moreover, chronological control of paleoenvironmental reconstructions in semi-arid Mongolia is often imprecise because chronologies are mostly derived from few ^{14}C -dates on bulk organic carbon. Bulk organic carbon has often been used in semi-arid regions since terrestrial macrofossils, which are assumed to be rapidly transported into the lake and thus are ideal for dating (Hajdas et al., 1995), are often absent. However, bulk organic carbon can be “pre-aged” because organic

material accumulates in the catchment over hundreds to thousands of years and possibly overestimates the “true” deposition age when ending up in the lake (Gierga et al., 2016; Douglas et al., 2018; Haas et al., 2019).

Here we present a continuous Holocene sediment record from Shireet Naiman Nuur (Nuur = lake), a high-altitude and endorheic lake with a small hydrological catchment in the central Mongolian Khangai Mountains. We aim to establish a robust chronology for the Shireet Naiman Nuur sediments by extensive ^{14}C -dating of bulk organic carbon and terrestrial macrofossils. To further evaluate and confirm the ^{14}C -based chronology, we use paleomagnetic secular variations, which we compare to predictions of geomagnetic field models for the coordinates of the coring location and the nearest regional sediment record which is from Lake Baikal. Lake sediment proxies, including elemental composition and bulk isotopes, were analyzed to characterize the Shireet Naiman Nuur sediments in greater detail and to infer changes in the lake's primary productivity as an indicator for changes in growing season temperature.

MATERIALS AND METHODS

Study Area

Shireet Naiman Nuur is a high-altitude lake in the central Mongolian Khangai Mountains ($46^{\circ}31'55.04''\text{N}$, $101^{\circ}49'16.23''\text{E}$; **Figure 1**). The lake is located at 2,429 m a.s.l. in the upper Orkhon Valley, where nomadic pastoralism has a long history (**Figures 1, 2A**). The lake's small hydrological catchment (~32.5 km²) with steep slopes reaches altitudes up to ~3,100 m a.s.l. Shireet Naiman Nuur has a length of ~3 km, a width of ~3.4 km and a maximum water depth of ~22.4 m. Currently, the lake has no outlet, i.e., it is endorheic, and the lake level is ~5 m below a potential overflow into the upper Orkhon Valley. The regional climate in the Khangai Mountains and at Shireet Naiman Nuur is characterized by long and cold winters dominated by the Siberian High, whereas 75% of the moisture is supplied by the mid-latitude Westerlies during the short summer from June to August (Tian et al., 2013; Chen et al., 2019). Today's mean annual temperature and precipitation at the nearest climate station Arvaikheer (CDC-ID 44388) is $2.0 \pm 0.9^{\circ}\text{C}$ and 256.4 ± 75.2 mm, respectively (period from 2009–2017; DWD Climate Center, 2021; **Figure 2B**). Because Shireet Naiman Nuur is located ~600 m higher than the nearest climate station at Arvaikheer, an even shorter growing season with lower mean annual temperatures can be expected. Consequently, the extreme environmental conditions at the lake lead to an ice cover prevailing 7 months per year from

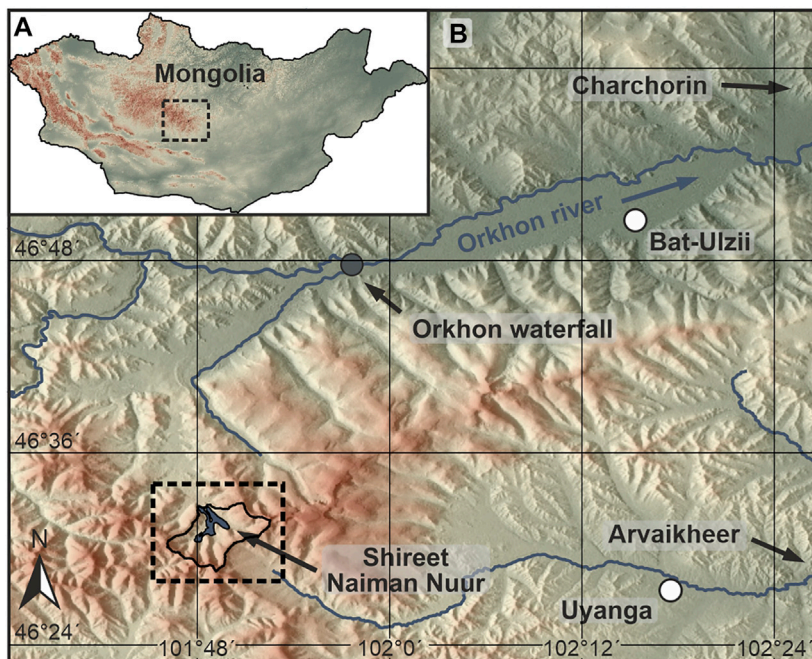


FIGURE 1 | Overview over the study area. **(A)** Mongolia with the black dotted rectangle indicating the Orkhon Valley in the southeastern Khangai Mountains. **(B)** The upper Orkhon Valley with Shireet Naiman Nuur and its catchment (i.e., black line, see **Figure 2** for blow up).

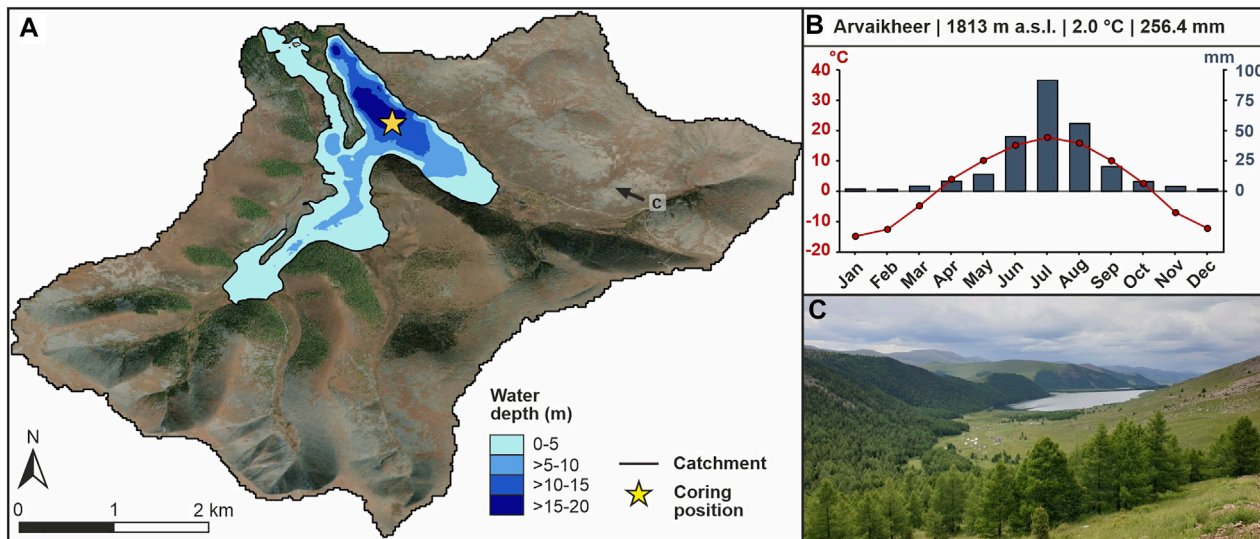


FIGURE 2 | Overview of the specific study area. **(A)** Bathymetric map of Shireet Naiman Nuur and satellite image of its catchment (bathymetry: own data, see **Supplementary Information SI 1** for more details; satellite image: Planet Team 2017). The coring location of the sediment core is indicated by the yellow star, the photograph and its viewing direction are also indicated. **(B)** Mean monthly temperature and precipitation of the nearest climate station Arvaikheer. **(C)** Photograph of the northern part of the Shireet Naiman Nuur catchment with *Larix sibirica* forests on the north-facing slopes.

November until May (2018-2020; Planet Team, 2017). The modern vegetation around the lake is dominated by grasses and steppe vegetation on the south-facing slopes, while the

north-facing slopes are vegetated by relatively dense *Larix sibirica* forest because of greater moisture availability (**Figure 2C**).

Sediment Core and Chronology

We retrieved a 178 cm long gravity core in summer 2019 from the deepest part of Shireet Naiman Nuur using an Uwitec gravity corer. The sediment core was split and photographed at the Friedrich Schiller University Jena. One half of the core was analyzed for elemental composition in 2 mm resolution using an X-ray fluorescence (XRF) scanner (Avaatech) at Eawag, Switzerland. The XRF scanner was sourced by an Oxford 100 W X-Ray tube with a rhodium anode and equipped with a Canberra X - PIPS/DSA 1000 (MCA) detector. The split core surface was carefully flattened for uniform scanning and covered with 4 µm Ultralene foil for avoiding contamination. Low elemental groups were measured at 10 kV (1500 A, no filter, 15 s exposure) and mid energy groups were measured at 30 kV (2000 A, Pd thin filter, 40 s exposure). Elemental data from XRF-scanning is presented as log ratios to eliminate sediment matrix effects, i.e., due to water content, surface roughness and grain size variations (Weltje and Tjallingii, 2008). After XRF scanning, a u-channel was taken from the identical core half for paleomagnetic analyses. The other half of the sediment core was subsampled at 1 cm intervals, freeze-dried and homogenized.

The chronology of the sediment core is based on ¹⁴C-dating of nine bulk organic carbon and 23 terrestrial macrofossil samples. For collecting terrestrial macrofossils, 1 cm slices of the half of the sediment core where the u-channel was taken, were wet sieved over a 200 µm sieve and terrestrial macrofossils were subsequently collected and identified. Prior to ¹⁴C-analyses, macrofossils and bulk organic carbon samples were treated with 1N HCl at 60°C for 8 h to remove carbonates. ¹⁴C-dating was carried out at the Laboratory for the Analysis of Radiocarbon with AMS at the University of Bern (Szidat et al., 2014), using a MIni CARbon DAting System (MICADAS) AMS coupled online to an Elementar Analyzer (Ruff et al., 2010; Wacker et al., 2010). ¹⁴C-results are reported as fraction modern (F¹⁴C) and were corrected for cross and constant contamination after Salazar et al. (2015). 10 tin boats were measured for constant contamination, which gave 1.5 µg C for a single boat with F¹⁴C values of 0.498. ¹⁴C-ages were calibrated to calendar ages using the IntCal20 calibration curve (Reimer et al., 2020). ¹⁴C-ages were then used to establish an age-depth model by Bayesian age modeling using the Bacon 2.3.4 package in R (Blaauw and Christen, 2011). To account for possible reservoir effects of the bulk organic carbon ¹⁴C-ages, we used the uppermost bulk organic carbon sample from 0–1 cm sediment depth, which gave a conventional ¹⁴C-age of 632 ± 101. This reservoir age was subtracted from all bulk organic carbon ¹⁴C-ages during Bayesian age modeling. One bulk organic carbon sample at 80 cm sediment depth and two terrestrial macrofossils at 29 and 79 cm sediment depth gave too old ¹⁴C-ages and were therefore excluded from Bayesian age modeling in a second iteration.

For paleomagnetic secular variations, natural remanent magnetization (NRM) was measured on the u-channel using stepwise (11 steps) alternating field (AF) demagnetization with peak AFs of 0, 5, 10, 15, 20, 30, 40, 50, 65, 80 and 100 mT. NRM was measured continuously at 1 cm intervals using a 2G Enterprise DC-4K liquid helium free magnetometer at GFZ Potsdam. The u-channel was split into two halves during sampling and paleomagnetic measurements on the u-channels were performed

in 1 cm steps extending 10 cm over both ends of the u-channel profiles with respect to the absolute depth scale. These data sets, on basis of the measured cartesian components (X,Y,Z), were then superimposed to compensate for the end-effect at the edges of the U-channels, thus yielding a continuous paleomagnetic record (Nowaczyk et al., 2020). Inclination and declination of the characteristic remanent magnetization (ChRM: in most cases 15–80 mT) and maximum angular deviation (MAD) were determined by principal component analyses (Kirschvink, 1980) and the median destructive field was also calculated. Declination data are relative since the azimuth could not be controlled during coring. Due to the width of the response function of the SQUID sensors, some smoothing occurs in the data. In order to eliminate edge effects, the upper- and lowermost 5 cm of the sequence are plotted in gray (Figure 3B).

Geochemical Analyses

Analyses for carbon and nitrogen contents, and the stable carbon isotopes were carried out with an Elementar Analyzer (vario EL cube) coupled to an isotope ratio mass spectrometer (Isoprime precision) in 1 cm resolution at the Friedrich Schiller University Jena. For total carbon (TC) and total nitrogen (N), ~10 mg of untreated sediment samples was weighed into tin boats and measured. For total organic carbon (TOC) and the carbon isotopic composition (δ¹³C_{TOC}), samples were treated with 1N HCl at 60°C for 8 h to remove carbonates. The samples were subsequently washed to pH neutrality with ultrapure water, and ~10 mg of sediment was weighted into tin boats for measurement. The analytical precision of the δ¹³C analyses was checked against certified standards (L-Proline, EDTA and USGS65), and gave an analytical error < 0.1‰. δ¹³C is given in its delta notation against the Vienna Pee Dee Belemnite (VPDB).

The molar TOC/N ratio was calculated based on their respective molecular weights as follows:

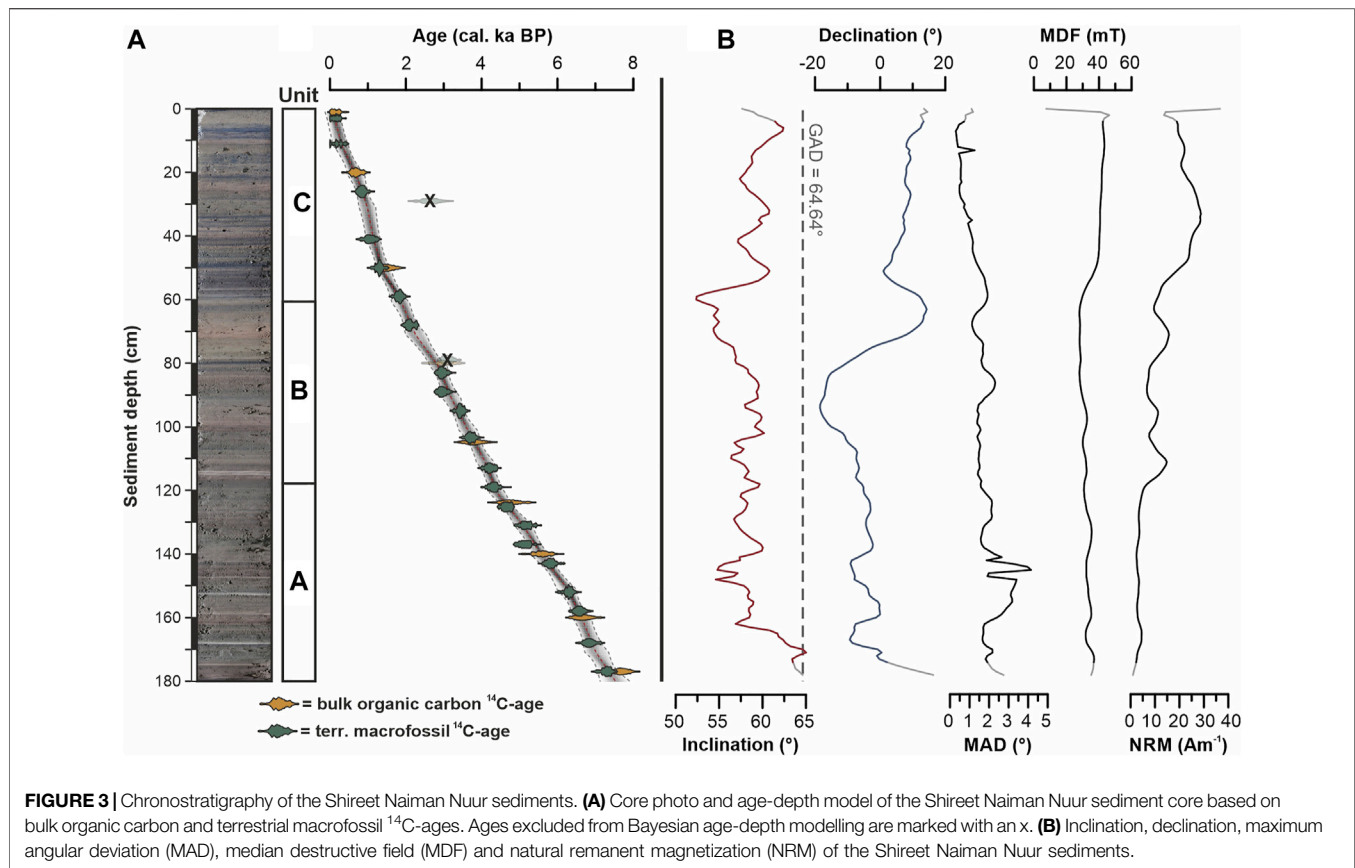
$$TOC/N[molar] = \frac{(TOC[\%] * 12.0107 [g * mol^{-1}])}{(N[\%] * 14.0067 [g * mol^{-1}])} \quad (1)$$

Pearson's r-values were calculated to detect correlations between the analyzed geochemical proxies and a student's t-test was used to check for significance (α < 0.05). Statistical analyses were carried out with the software OriginPro 2022.

RESULTS

Lithostratigraphy and Chronology

The 178 cm long sediment core from Shireet Naiman Nuur comprises mostly layered sediments of fine- to medium-grained silty material (see **Supplementary Information SI 2** for grain size analyses and results) and shows three lithological units based on differences in sediment color and geochemical properties. In Unit A (from 178 to 118 cm), two pale layers at 167 and 152 cm sediment depth interrupt the brownish and well laminated sediments. The brownish layered sediments in Unit B (from 118 to 60 cm) are interrupted by a double pale layer at 114 cm sediment depth,



and blackish sediments at 80 cm sediment depth. In Unit C (from 60 to 0 cm), another pale layer occurs at 59 cm sediment depth and well laminated brownish sediments contain intercalated blackish layered sediments (Figure 3A).

Bayesian age-depth modeling of ^{14}C -dated bulk organic carbon samples and terrestrial macrofossils (see **Supplementary Information SI 3** for detailed ^{14}C -dating results) gave a modeled basal median ^{14}C -age of 7.4 ± 0.3 cal ka BP. All ^{14}C -ages are in stratigraphic order, except for a terrestrial macrofossil sample at 29 cm, which shows a large offset to the other ages, as well as a bulk organic carbon sample at 80 cm and another terrestrial macrofossil sample at 79 cm, which are slightly too old for their stratigraphic position but still within the modelled 2σ error (Figure 3A). The reservoir corrected bulk organic carbon ^{14}C -ages correspond very well with the ^{14}C -ages of the terrestrial macrofossils.

NRM intensities range from 2.4 to 28.8 Am^{-1} and MDF values from 27.9 to 43.3 mT . Inclination and declination show distinct changes (Figure 3B). Inclination ranges from 52 to 65°N and only intersects the one expected, based on a geocentric axial dipole model ($\text{GAD} = 64.64^\circ$), in the lowermost part of the record. Such a flattened inclination compared to the GAD has been often noticed in sediments and has been attributed to compaction processes (Henkel et al., 2016). Declination stretches over 32° , which in general is typical for paleomagnetic secular variations (Haberzettl et al., 2015; Haberzettl et al., 2021). Well preserved and stable single-component magnetization is indicated by low

MAD values (Stoner and St-Onge, 2007) that are generally below 4.1° .

Geochemical Results

TOC and N contents range from 4.5 to 10.6% and 0.6 – 1.4% , respectively, with generally higher values in Unit A (i.e., from 178 to 118 cm), a decreasing trend in Unit B (i.e., from 118 to 60 cm) and lower values in Unit C (i.e., from 60 to 0 cm ; Figure 4). The molar TOC/N ratio shows values between 5.4 and 7.9 , covering only a very small range. The pattern of TOC and N is resembled by $\log(\text{Ca}/\text{Ti})$ and $\log(\text{Si}/\text{Ti})$ values that are likewise higher in Unit A, show a decreasing trend in Unit B and lower values in Unit C. Abrupt decreases in TOC, N, $\log(\text{Ca}/\text{Ti})$ and $\log(\text{Si}/\text{Ti})$ are notable at 167 , 152 , 114 and 59 cm sediment depth, corresponding to the four macroscopically detected pale layers (Figure 4). $\delta^{13}\text{C}_{\text{TOC}}$ values range from -31.4 to -27.9% and are more negative in Unit A, variable in Unit B and more positive in Unit C (Figure 4).

Correlations of the geochemical proxies are all significant (Table 1). TOC, N, $\log(\text{Ca}/\text{Ti})$ and $\log(\text{Si}/\text{Ti})$ are positively correlated with each other, but negatively correlated to $\delta^{13}\text{C}_{\text{TOC}}$.

DISCUSSION

Chronology

Extensive ^{14}C -dating of the finely layered silty sediments from Shireet Naiman Nuur allows us to establish a robust and precise

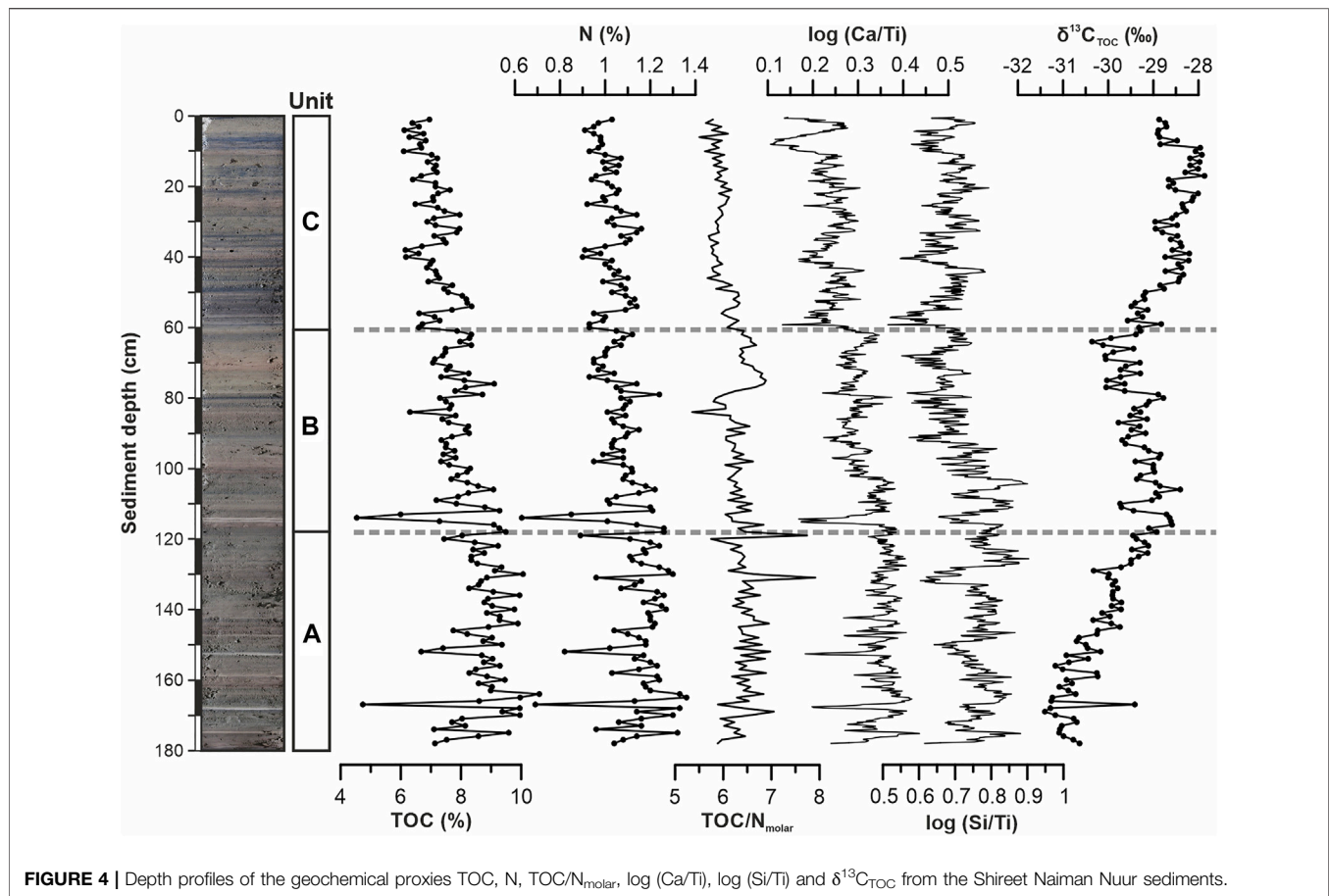


FIGURE 4 | Depth profiles of the geochemical proxies TOC, N, TOC/N_{molar}, log (Ca/Ti), log (Si/Ti) and $\delta^{13}\text{C}_{\text{TOC}}$ from the Shireet Naiman Nuur sediments.

TABLE 1 | Correlation matrix (Person's *r*) of the geochemical proxies from Shireet Naiman Nuur.

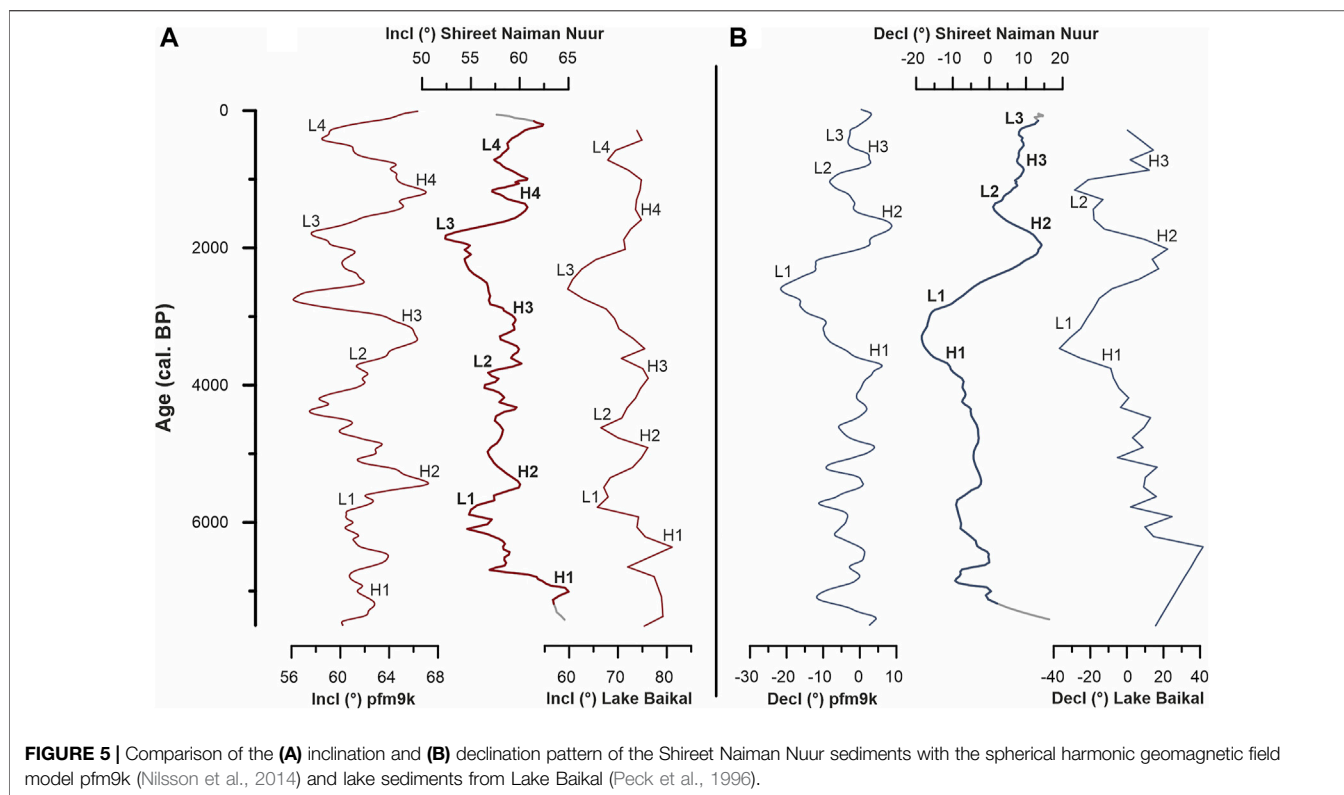
<i>n</i> = 178	N (%)	log (Ca/Ti)	log (Si/Ti)	$\delta^{13}\text{C}_{\text{TOC}}$ (‰)
TOC (%)	0.91	0.65	0.51	-0.60
N (%)		0.51	0.46	-0.45
log (Ca/Ti)			0.75	-0.63
log (Si/Ti)				-0.34

Bold values indicate significance ($\alpha < 0.05$).

chronology for the past 7.4 ± 0.3 cal ka BP (Figure 3A). While almost all ^{14}C -ages are in stratigraphic order, the terrestrial macrofossil sample at 29 cm sediment depth is pre-aged and has an age-offset of $\sim 1,500$ years. Although the median ^{14}C -age of the bulk organic carbon sample and the terrestrial macrofossil sample at 80 and 79 cm sediment depth are still within the modelled 2σ error, they have a slight age-offset of ~ 250 years and are likewise slightly pre-aged (Figure 3A). Those pre-aged samples probably represent reworked and mobilized organic material that has been stored in the catchment soils for a certain time before final erosion (Haberzettl et al., 2013; Gierga et al., 2016; Bliedtner et al., 2020). They therefore overestimate their “true” burial age and we excluded them from age-depth modeling. However, all remaining ^{14}C -ages are

stratigraphically very consistent and indicate that residence times of organic material in the catchment soils and transfer times through the catchment are very short and negligible. Moreover, the temporal resolution of our core derived from Bayesian age modeling is 16 (i.e., in the upper part) to 72 years (i.e., in the lower part) per centimeter sediment, which correspond to a decadal to centennial temporal resolution.

The ^{14}C -based chronology from Shireet Naiman Nuur is further confirmed by paleomagnetic secular variation stratigraphy. Observed variations in inclination correspond very well with outputs of various spherical harmonic geomagnetic field models. A comparison to the pfm9k model (Nilsson et al., 2014) is shown in Figure 5, which showed the best resemblance. Slight offsets are within the ^{14}C -dating uncertainties of the Shireet Naiman Nuur sediments. Compared to the closest regional paleomagnetic secular variation record from Lake Baikal (Peck et al., 1996), the Baikal inclination pattern shows similar features to Shireet Naiman Nuur and the pfm9k inclination pattern (Figure 5A), but less obviously and sometimes with an offset in timing. Nevertheless, the overall trend of the inclination pattern at Lake Baikal follows that of our record and the pfm9k model during the past 7.4 ka. Discrepancies in the inclination pattern of Lake Baikal compared to Shireet Naiman Nuur and the pfm9k model might be explained by small-scale regional differences in the drift of the non-dipole field (Merrill et al.,



1996). However, they could also be explained by possible uncertainties in the Lake Baikal chronology, that is, mostly based on ^{14}C -dated bulk organic carbon (Colman et al., 1996; Peck et al., 1996). Although the ^{14}C -ages are reservoir corrected by dated surficial sediments, changes in the discharge of the Selenga River into Lake Baikal could have strongly influenced sedimentation rates and transfer times of organic material deposited in the analyzed sediment cores located in front of the Selenga delta. Comparing the declination pattern recorded in the Shireet Naiman Nuor and Lake Baikal sediments over the past 7.4 ka, both records resemble very well the declination pattern of the pfm9k model (Peck et al., 1996; Nilsson et al., 2014). Especially since ~ 4 ka, three distinct declination lows and highs are recorded, although H1 and L1 appear a bit earlier in the Shireet Naiman Nuor and Lake Baikal record compared to the pfm9k model (Figure 5B).

Overall, inclination and declination patterns recorded in the Shireet Naiman Nuor sediments are in very good agreement with the pfm9k model of Nilsson et al. (2014). Therefore, paleomagnetic secular variations validate and confirm our extensively dated ^{14}C -chronology, providing a very robust age control for the 7.4 ka lake sediments from Shireet Naiman Nuor. Moreover, our robustly dated paleomagnetic secular variation record can serve as a valuable regional master record for using paleomagnetic secular variation stratigraphy in semi-arid Mongolia as a powerful tool to evaluate and refine ^{14}C -chronologies. This is especially important since terrestrial macrofossils are often absent in semi-arid lake sediments and bulk organic carbon

can have large residence and transfer times in and through the catchment.

Lake Primary Productivity

Changes in TOC in the Shireet Naiman Nuor sediments are interpreted in terms of lake primary productivity. The higher TOC values in Unit A followed by the trend to lower values in Unit B and the lower values in Unit C indicate a trend from increased to low primary productivity in the Shireet Naiman Nuor sediments (Figure 4). TOC is a well-known indicator for primary productivity in lacustrine sediments if organic material is mainly derived from aquatic biogenic producers (Haberzettl et al., 2005; Kasper et al., 2015; Zhu et al., 2015), which is suggested for the Shireet Naiman Nuor sediments by low molar TOC/N ratios < 8 (Meyers, 2003). TOC is additionally resembled by N, $\log(\text{Ca}/\text{Ti})$ and $\log(\text{Si}/\text{Ti})$, and their significant correlation with TOC ($r = 0.91, 0.65$ and 0.51 , respectively; $\alpha < 0.05$; Table 1) suggesting that they are also indicative for changes in lake primary productivity in the Shireet Naiman Nuor sediments. We acknowledge that Ca and Si could also originate from geogenic sources from the catchment or productivity independent precipitation processes. However, due to the significant correlations to TOC and N, $\log(\text{Ca}/\text{Ti})$ and $\log(\text{Si}/\text{Ti})$ ratios are similarly interpreted. Changes in primary productivity in high-altitude and high-latitude lakes in turn are mainly controlled by growing season temperatures because the duration of ice-cover and the growing season of aquatic producers is strongly determined by air temperatures (Willemse and Törnqvist, 1999; Mischke et al., 2010). Recently, such a relationship was also found for the past 4.2 ka in the high-

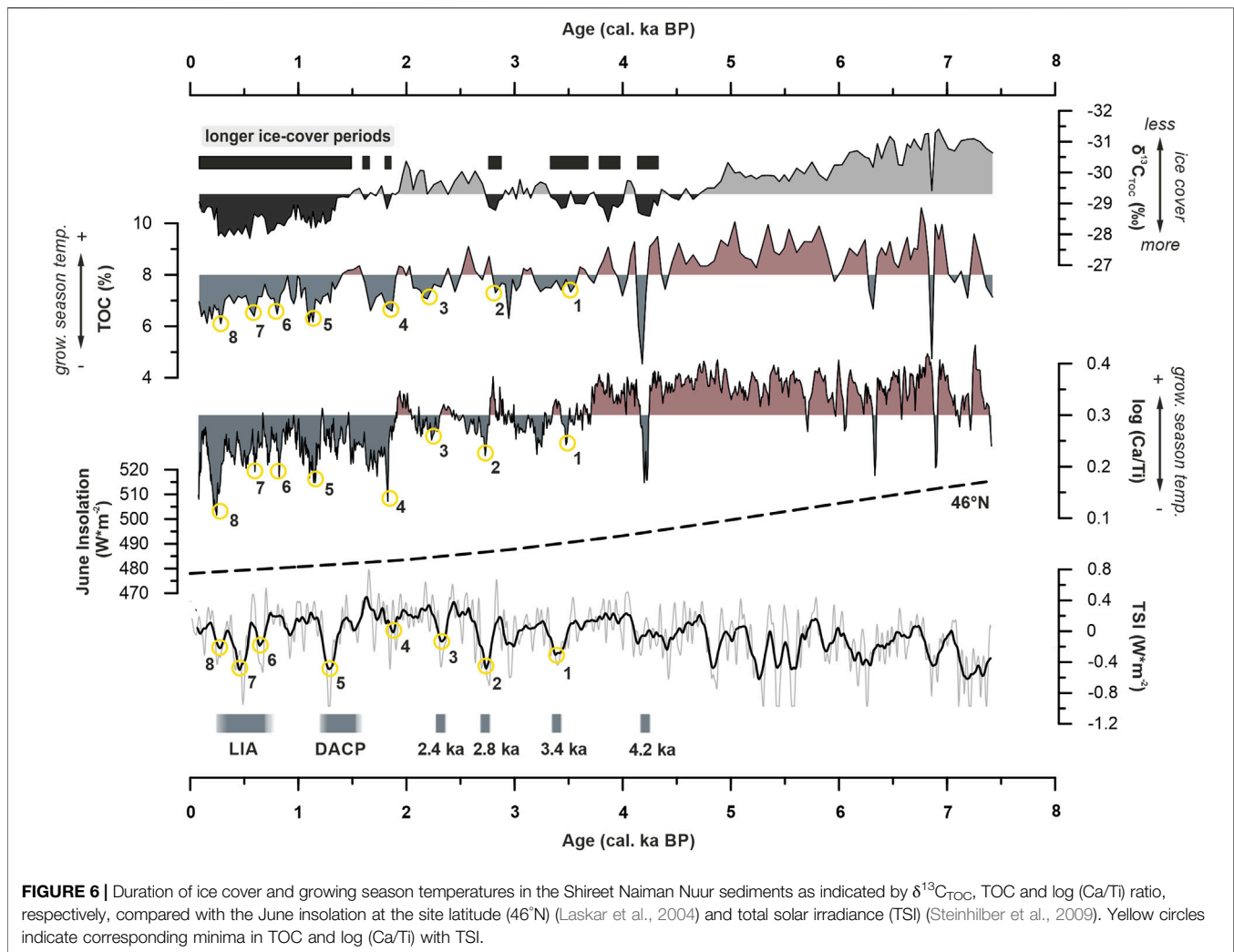


FIGURE 6 | Duration of ice cover and growing season temperatures in the Shireet Naiman Nuur sediments as indicated by $\delta^{13}\text{C}_{\text{TOC}}$, TOC and $\log(\text{Ca/Ti})$ ratio, respectively, compared with the June insolation at the site latitude (46°N) (Laskar et al., 2004) and total solar irradiance (TSI) (Steinhilber et al., 2009). Yellow circles indicate corresponding minima in TOC and $\log(\text{Ca/Ti})$ with TSI.

altitude lake sediments of Khar Nuur which is located in the Mongolian Altai and has a comparable environmental setting (Bliedtner et al., 2021). According to this interpretation, lake primary productivity and growing season temperatures at Shireet Naiman Nuur were high in Unit A from 7.4 ± 0.3 to 4.3 ± 0.2 cal ka BP, decreasing in Unit B from 4.3 ± 0.2 to 1.9 ± 0.2 cal ka BP and lowest in Unit C from 1.9 ± 0.2 cal ka BP until present day (Figures 4, 6). The abrupt decreases of lake primary productivity in the pale layers at 167 cm (6.9 ± 0.3 cal ka BP), 152 cm (6.3 ± 0.2 cal ka BP), 114 cm (4.2 ± 0.2 cal ka BP) and 59 cm (1.8 ± 0.2 cal ka BP) sediment depth probably document increased minerogenic input from erosive events, possibly induced by rapid climate changes (Figures 4, 6).

Lower growing season temperatures and longer ice cover periods in Unit C (i.e., from 1.9 ± 0.2 cal ka BP until present day) are supported by more positive $\delta^{13}\text{C}_{\text{TOC}}$ values (Figure 4). Since organic material in the Shireet Naiman Nuur sediments is mainly derived from aquatic biogenic production (see low molar TOC/N ratios), the $\delta^{13}\text{C}_{\text{TOC}}$ signal mainly indicates the dissolved inorganic carbon (DIC) sources aquatic producers use for

biosynthesis. $\delta^{13}\text{C}_{\text{TOC}}$ values are more negative if aquatic producers use dissolved CO_2 from the water column, that is, in equilibrium with the atmosphere ($\delta^{13}\text{C} = \sim -7\text{‰}$). In contrast, $\delta^{13}\text{C}_{\text{TOC}}$ values become more positive when dissolved CO_2 is limited and exhausted, and aquatic producers begin to use dissolved bicarbonates (HCO_3^-) ($\delta^{13}\text{C} = \sim -1\text{‰}$) (Meyers, 2003). In most cases enhanced primary productivity results in the consumption of dissolved CO_2 and the incorporation of dissolved HCO_3^- (Meyers, 2003; Leng and Marshall, 2004; Lamb et al., 2006), but in high-altitude and high-latitude lakes also ice cover can determine the availability of dissolved CO_2 (Striegl et al., 2001; Neumann et al., 2004). Studies of high-latitude lakes showed that a shortening of the ice cover period results in longer mixing of the lake during spring with a slower rate until summer stratification sets in, and vice versa if the ice cover period was longer (Couture et al., 2015; Pilla and Williamson, 2021). Therefore, we suggest at Shireet Naiman Nuur, where ice coverage is in the order of 7 months, that more dissolved CO_2 is available during shorter ice periods with longer mixing, resulting in more negative $\delta^{13}\text{C}_{\text{TOC}}$ values,

i.e., from 7.4 ± 0.3 to 4.3 ± 0.2 (Figure 6). In contrast, dissolved CO_2 becomes exhausted during longer ice cover periods with shorter mixing, resulting in beginning incorporation of dissolved HCO_3^- and more positive $\delta^{13}\text{C}_{\text{TOC}}$ values, i.e., from 1.9 ± 0.2 cal ka BP until present day. Variable $\delta^{13}\text{C}_{\text{TOC}}$ values from 4.3 ± 0.2 to 1.9 ± 0.2 cal ka BP indicate changing dissolved DIC sources due to changes in ice cover periods (Figure 6). Lower growing season temperatures and longer ice cover periods are further supported by the significant negative correlation of the lake primary productivity indices TOC and $\log(\text{Ca}/\text{Ti})$ with $\delta^{13}\text{C}_{\text{TOC}}$ ($r = -0.60$ and -0.63 , respectively; $\alpha < 0.05$; Table 1).

Therefore, increased primary productivity and higher growing season temperatures occurred at Shireet Naiman Nuur during the Middle Holocene from 7.4 ± 0.3 to 4.3 ± 0.2 cal ka BP. Lower growing season temperatures and longer ice cover periods occurred during the Late Holocene from 4.3 ± 0.2 cal ka BP until present day (Figure 6).

Paleoenvironmental Implications

The overall pattern of higher growing season temperatures at Shireet Naiman Nuur during the Middle Holocene seem to be driven by higher summer insolation (Figure 6). Strong summer solar heating, Arctic temperature amplification and sea ice loss was reported for mid- and high-latitudes of the Northern Hemisphere for the Middle Holocene, resulting in the “Holocene thermal maximum” and a pronounced warming (Wanner et al., 2008; Renssen et al., 2009; Park et al., 2019). Especially for mid-latitude Central Asia, increased summer temperatures between ~ 8 and 4 ka BP were recently reported to be insolation-driven by a compiled temperature index of Lan et al. (2021). With the onset of neoglaciation ~ 4 ka BP due to reducing summer insolation, colder temperatures prevailed during the Late Holocene (Zhao et al., 2017; Lan et al., 2021), which is also evident at Shireet Naiman Nuur during the past 4.3 ± 0.2 cal ka BP (Figure 6). Although growing season temperatures overall started to decrease since then, an abrupt decrease in growing season temperatures at 4.2 ± 0.2 cal ka BP is notable and exceptional in our record. This abrupt cooling likely indicating an event of rapid climate change at Shireet Naiman Nuur and coincides with the 4.2 ka event, a period of cold conditions probably related to enhanced ice-rafted debris in the northern North Atlantic (Bond et al., 2001). Unfortunately, it was not yet possible to attribute the other pronounced minima in our productivity indicators at 6.9 ± 0.3 and 6.3 ± 0.2 cal ka BP to more widely known climate anomalies.

While summer insolation generally decreased during the Late Holocene, variations in growing season temperatures at Shireet Naiman Nuur during that time might be modulated by total solar irradiance (TSI) (Steinhilber et al., 2009). Although we have to note that the timing of growing season minima slightly differs from minima in TSI, they are still within our chronologies 2σ error. Moreover, the magnitude of changes in the productivity indices should rather be considered as relative changes because of site-specific and matrix effects, and therefore do not necessarily reflect the same magnitude of changes in TSI. Nevertheless, abrupt changes to lower growing season temperatures occur at Shireet Naiman Nuur during minima in TSI at $\sim 3.4, 2.8, 2.4$ cal ka

BP. A strong cooling starts ~ 1.8 cal ka BP and lasts until ~ 1 cal ka BP (Figure 6). This cooling phase includes the Dark Ages Cold Period (DACP) and/or Late Antique Little Ice Age (LALIA) from ~ 1.6 to 1.2 ka BP (Büntgen et al., 2016; Helama et al., 2017). Compared to Mongolian lowland records (Yang et al., 2020; Rudaya et al., 2021; Struck et al., 2022), the following Medieval Climate Anomaly (MCA) does not appear that pronounced as a warm period in the Shireet Naiman Nuur sediments. However, colder conditions are evident during the Little Ice Age (LIA) and growing season temperatures especially decrease during the Maunder Minima (Figure 6).

The insolation-driven trend of warmer growing season conditions during the Middle Holocene to colder growing season conditions during the Late Holocene since 4.3 ± 0.2 cal ka BP is also reflected in several pollen reconstructions from central and northern Mongolia (Fowell et al., 2003; Prokopenko et al., 2007; Wang et al., 2011; Unkelbach et al., 2021). The TSI controlled variation in growing season temperatures at Shireet Naiman Nuur during the Late Holocene was previously described for another high-altitude site from the Mongolian Altai (Bliedtner et al., 2021). Although the MCA is not that pronounced in both records, they well reflect the Late Holocene climate anomalies that were also regionally reported from pollen reconstructions (Yang et al., 2020; Rudaya et al., 2021), a glycerol dialkyl glycerol tetraether based temperature reconstruction (Dugerdil et al., 2021) and an isotope based moisture reconstruction (Struck et al., 2022).

CONCLUSION

Our study presents a continuous 7.4 ka sediment record from the high-altitude Shireet Naiman Nuur in the central Mongolian Khangai Mountains. Our chronological approach and sedimentological analyses gave the following results:

- We established a robust and precise chronology of the layered silty Shireet Naiman Nuur sediments by extensive ^{14}C -dating of 23 terrestrial macrofossils and nine bulk organic carbon samples. Bayesian age modeling gave a basal modeled median age of 7.4 ± 0.3 cal ka BP, and mostly all ^{14}C -ages are in stratigraphic order. The ^{14}C -based chronology of the Shireet Naiman Nuur sediments is evaluated and confirmed by paleomagnetic secular variation that resemble the spherical harmonic geomagnetic field model pfm9k. The very good and robust age control of the Shireet Naiman Nuur chronology makes paleomagnetic secular variation stratigraphy a powerful tool in semi-arid Mongolia for evaluating and refining ^{14}C -chronologies when compared to our record.
- The lake sediment proxies TOC, N, $\log(\text{Ca}/\text{Ti})$ and $\log(\text{Si}/\text{Ti})$ reveal increased lake primary productivity and higher growing season temperatures from 7.4 ± 0.3 to 4.3 ± 0.2 cal ka BP and reduced productivity and lower growing season temperatures thereafter. Lower lake primary productivity and growing season temperatures are likely the result of longer ice-cover periods at the high-altitude Shireet Naiman

Nuur. This is supported by $\delta^{13}\text{C}_{\text{TOC}}$, which is more positive during increased ice cover periods because of shorter mixing periods of the lake water and the preferential incorporation of dissolved HCO_3^- by aquatic producers after dissolved CO_2 becomes exhausted and limited.

- Higher growing season temperatures at Shireet Naiman Nuur during the Middle Holocene (i.e., from 7.4 ± 0.3 to 4.3 ± 0.2 cal ka BP) are mainly the result of stronger summer insolation during that time and pronounced warming. Reducing summer insolation during the Late Holocene results in lower growing season temperatures at Shireet Naiman Nuur from 4.3 ± 0.2 cal ka BP until present day and the globally acknowledged 4.2 ka event also appears at Shireet Naiman Nuur as an abrupt and pronounced cooling event. While growing season temperatures are generally decreased during the Late Holocene, variations are controlled by TSI. Abrupt cooling occurred during minima in TSI at ~ 3.4 , 2.8 and 2.4 cal ka BP and more long-lasting and pronounced cooling starts ~ 1.8 cal ka BP and lasts during the Dark Ages Cold Period and the Little Ice Age.

Based on our results, Shireet Naiman Nuur provides a valuable continuous sediment archive for the past 7.4 ka with a very precise chronological control. Future studies from the region can use paleomagnetic secular variations to validate and refine their ^{14}C -based chronologies when compared with our newly obtained record and allow a radiocarbon chronology independent comparison of paleoclimate proxies. Moreover, the Shireet Naiman Nuur sediments provide a robust base for future paleoenvironmental and paleoclimatic reconstructions by, e.g., biomarker and pollen analyses.

DATA AVAILABILITY STATEMENT

The original contributions presented in the study are included in the article/**Supplementary Material**, further inquiries can be directed to the corresponding author.

REFERENCES

- Aizen, E. M., Aizen, V. B., Melack, J. M., Nakamura, T., and Ohta, T. (2001). Precipitation and Atmospheric Circulation Patterns at Mid-latitudes of Asia. *Int. J. Climatol.* 21, 535–556. doi:10.1002/joc.626
- Blaauw, M., and Christen, J. A. (2011). Flexible Paleoclimate Age-Depth Models Using an Autoregressive Gamma Process. *Bayesian Anal.* 6, 457–474. doi:10.1214/11-BA61810.1214/ba/1339616472
- Bliedtner, M., Struck, J., Strobel, P., Salazar, G., Szidat, S., Bazarradnaa, E., et al. (2021). Late Holocene Climate Changes in the Altai Region Based on a First High-Resolution Biomarker Isotope Record from Lake Khar Nuur. *Geophys. Res. Lett.* 48 (20), e2021GL094299. doi:10.1029/2021GL094299
- Bliedtner, M., von Suchodoletz, H., Schäfer, I., Welte, C., Salazar, G., Szidat, S., et al. (2020). Age and Origin of Leaf Wax nC_{29} -Alkanes in Fluvial Sediment-Paleosol Sequences and Implications for Paleoenvironmental Reconstructions. *Hydrol. Earth Syst. Sci.* 24, 2105–2120. doi:10.5194/hess-24-2105-2020

AUTHOR CONTRIBUTIONS

MB: Conceptualization, Formal analysis, Funding acquisition, Investigation, Writing—original draft, Writing—review and editing, PS: Conceptualization, Investigation, Writing—review and editing, JS: Conceptualization, Writing—review and editing, GS: Investigation, Writing—review and editing, SS: Writing—review and editing, NN: Investigation, Writing—review and editing, EB: Writing—review and editing, RL: Investigation, Writing—review and editing, ND: Writing—review and editing, TH: Investigation, Writing—review and editing, RZ: Conceptualization, Writing—review and editing.

FUNDING

This study was funded by the German Research Foundation DFG (BL 1781/2-1).

ACKNOWLEDGMENTS

We would like to thank the Ernst Abbe Stiftung for financial support of the field trip to Mongolia and sediment retrieval. We further thank our logistic partners in Mongolia for their support during fieldwork. PS gratefully acknowledges the support by a fellowship from the state of Thuringia (Landesgraduiertenstipendium). Especially acknowledged are T. Henning, J. Löhrlin, and M. Wagner for support during laboratory work. We thank two reviewers for their valuable and helpful comments on this paper.

SUPPLEMENTARY MATERIAL

The Supplementary Material for this article can be found online at: <https://www.frontiersin.org/articles/10.3389/feart.2022.910782/full#supplementary-material>

- Bond, G., Kromer, B., Beer, J., Muscheler, R., Evans, M. N., Showers, W., et al. (2001). Persistent Solar Influence on North Atlantic Climate during the Holocene. *Science* 294, 2130–2136. doi:10.1126/science.1065680
- Brugger, S. O., Gobet, E., Sigl, M., Osmont, D., Papina, T., Rudaya, N., et al. (2018). Ice Records Provide New Insights into Climatic Vulnerability of Central Asian Forest and Steppe Communities. *Glob. Planet. Change* 169, 188–201. doi:10.1016/j.gloplacha.2018.07.010
- Büntgen, U., Myglan, V. S., Ljungqvist, F. C., McCormick, M., Di Cosmo, N., Sigl, M., et al. (2016). Cooling and Societal Change during the Late Antique Little Ice Age from 536 to Around 660 AD. *Nat. Geosci.* 9, 231–236. doi:10.1038/ngeo2652
- Chen, F., Chen, J., Huang, W., Chen, S., Huang, X., Jin, L., et al. (2019). Westerlies Asia and Monsoonal Asia: Spatiotemporal Differences in Climate Change and Possible Mechanisms on Decadal to Sub-orbital Timescales. *Earth-Science Rev.* 192, 337–354. doi:10.1016/j.earscirev.2019.03.005
- Colman, S. M., Jones, G. A., Rubin, M., King, J. W., Peck, J. A., and Orem, W. H. (1996). AMS Radiocarbon Analyses from Lake Baikal, Siberia: Challenges of Dating Sediments from a Large, Oligotrophic Lake. *Quat. Sci. Rev.* 15, 669–684. doi:10.1016/0277-3791(96)00027-3

- Couture, R. M., Wit, H. A., Tominaga, K., Kiuru, P., and Markelov, I. (2015). Oxygen Dynamics in a Boreal Lake Responds to Long-term Changes in Climate, Ice Phenology, and DOC Inputs. *J. Geophys. Res. Biogeosci.* 120, 2441–2456. doi:10.1002/2015JG003065
- Crutzen, P. J. (2002). Geology of Mankind. *Nature* 415, 23. doi:10.1038/415023a
- D'Arrigo, R., Jacoby, G., Pederson, N., Frank, D., Buckley, B., Nachin, B., et al. (2000). Mongolian Tree-Rings, Temperature Sensitivity and Reconstructions of Northern Hemisphere Temperature. *Holocene* 10, 669–672. doi:10.1191/09596830094926
- Dai, A. (2011). Drought under Global Warming: A Review. *WIREs Clim. Change* 2, 45–65. doi:10.1002/wcc.81
- Douglas, P. M. J., Pagani, M., Eglinton, T. I., Brenner, M., Curtis, J. H., Breckenridge, A., et al. (2018). A Long-Term Decrease in the Persistence of Soil Carbon Caused by Ancient Maya Land Use. *Nat. Geosci.* 11, 645–649. doi:10.1038/s41561-018-0192-7
- Dugerdil, L., Ménot, G., Peyron, O., Jouffroy-Bapicot, I., Ansanay-Alex, S., Antheaume, I., et al. (2021). Late Holocene Mongolian Climate and Environment Reconstructions from brGDGTs, NPPs and Pollen Transfer Functions for Lake Ayrag: Paleoclimate Implications for Arid Central Asia. *Quat. Sci. Rev.* 273, 107235. doi:10.1016/j.quascirev.2021.107235
- Fernández-Giménez, M. E., Venable, N. H., Angerer, J., Fassnacht, S. R., Reid, R. S., and Khishigbayar, J. (2017). Exploring Linked Ecological and Cultural Tipping Points in Mongolia. *Anthropocene* 17, 46–69. doi:10.1016/j.ancene.2017.01.003
- Fowell, S. J., Hansen, B. C. S., Peck, J. A., Khosbayar, P., and Ganbold, E. (2003). Mid to Late Holocene Climate Evolution of the Lake Telmen Basin, North Central Mongolia, Based on Palynological Data. *Quat. Res.* 59, 353–363. doi:10.1016/S0033-5894(02)00020-0
- Gierga, M., Hajdas, I., van Raden, U. J., Gilli, A., Wacker, L., Sturm, M., et al. (2016). Long-stored Soil Carbon Released by Prehistoric Land Use: Evidence from Compound-specific Radiocarbon Analysis on Soppensee Lake Sediments. *Quat. Sci. Rev.* 144, 123–131. doi:10.1016/j.quascirev.2016.05.011
- Haas, M., Baumann, F., Castella, D., Haghipour, N., Reusch, A., Strasser, M., et al. (2019). Roman-driven Cultural Eutrophication of Lake Murten, Switzerland. *Earth Planet. Sci. Lett.* 505, 110–117. doi:10.1016/j.epsl.2018.10.027
- Haberzettl, T., Fey, M., Lücke, A., Maidana, N., Mayr, C., Ohlendorf, C., et al. (2005). Climatically Induced Lake Level Changes during the Last Two Millennia as Reflected in Sediments of Laguna Potrok Aike, Southern Patagonia (Santa Cruz, Argentina). *J. Paleolimnol.* 33, 283–302. doi:10.1007/s10933-004-5331-z
- Haberzettl, T., Henkel, K., Kasper, T., Ahlborn, M., Su, Y., Wang, J., et al. (2015). Independently Dated Paleomagnetic Secular Variation Records from the Tibetan Plateau. *Earth Planet. Sci. Lett.* 416, 98–108. doi:10.1016/j.epsl.2015.02.007
- Haberzettl, T., Kasper, T., Stoner, J. S., Rahobisoa, J. J., and Daut, G. (2021). Extending and Refining the Paleomagnetic Secular Variation Database for South-Eastern Africa (Madagascar) to 2500 Cal BP. *Earth Planet. Sci. Lett.* 565, 116931. doi:10.1016/j.epsl.2021.116931
- Haberzettl, T., St-Onge, G., Behling, H., and Kirleis, W. (2013). Evaluating Late Holocene Radiocarbon-Based Chronologies by Matching Palaeomagnetic Secular Variations to Geomagnetic Field Models: an Example from Lake Kalimpa (Sulawesi, Indonesia). *Geol. Soc. Lond. Spec. Publ.* 373, 245–259. doi:10.1144/SP373.10
- Hajdas, I., Bonani, G., and Goslar, T. (1995). Radiocarbon Dating the Holocene in the Gościąg Lake Floating Varve Chronology. *Radiocarbon* 37, 71–74. doi:10.1017/S0033822200014806
- Helama, S., Jones, P. D., and Briffa, K. R. (2017). Dark Ages Cold Period: A Literature Review and Directions for Future Research. *Holocene* 27, 1600–1606. doi:10.1177/0959683617693898
- Henkel, K., Haberzettl, T., St-Onge, G., Wang, J., Ahlborn, M., Daut, G., et al. (2016). High-resolution Paleomagnetic and Sedimentological Investigations on the Tibetan Plateau for the Past 16 Ka Cal B.P.-The Tangra Yumco Record. *Geochim. Geophys. Geosyst.* 17, 774–790. doi:10.1002/2015GC006023
- Hoerling, M. P., Hurrell, J. W., and Xu, T. (2001). Tropical Origins for Recent North Atlantic Climate Change. *Science* 292, 90–92. doi:10.1126/science.1058582
- Huang, X., Peng, W., Rudaya, N., Grimm, E. C., Chen, X., Cao, X., et al. (2018). Holocene Vegetation and Climate Dynamics in the Altai Mountains and Surrounding Areas. *Geophys. Res. Lett.* 45, 6628–6636. doi:10.1029/2018GL078028
- IPCC (2021). *Climate Change 2021: The Physical Science Basis. Contribution of Working Group I to the Sixth Assessment Report of the Intergovernmental Panel on Climate Change*. Cambridge, UK: Cambridge University Press.
- Kasper, T., Haberzettl, T., Wang, J., Daut, G., Doberschütz, S., Zhu, L., et al. (2015). Hydrological Variations on the Central Tibetan Plateau since the Last Glacial Maximum and Their Teleconnection to Inter-regional and Hemispheric Climate Variations. *J. Quat. Sci.* 30, 70–78. doi:10.1002/jqs.2759
- Kirschvink, J. L. (1980). The Least-Squares Line and Plane and the Analysis of Palaeomagnetic Data. *Geophys. J. Int.* 62, 699–718. doi:10.1111/j.1365-246X.1980.tb02601.x
- Lamb, A. L., Wilson, G. P., and Leng, M. J. (2006). A Review of Coastal Palaeoclimate and Relative Sea-Level Reconstructions Using $\delta^{13}\text{C}$ and C/N Ratios in Organic Material. *Earth-Science Rev.* 75, 29–57. doi:10.1016/j.earscirev.2005.10.003
- Lan, J., Wang, T., Dong, J., Kang, S., Cheng, P., Zhou, K. e., et al. (2021). The Influence of Ice Sheet and Solar Insolation on Holocene Moisture Evolution in Northern Central Asia. *Earth-Science Rev.* 217, 103645. doi:10.1016/j.earscirev.2021.103645
- Laskar, J., Robutel, P., Joutel, F., Gastineau, M., Correia, A. C. M., and Levrard, B. (2004). A Long-Term Numerical Solution for the Insolation Quantities of the Earth. *A&A* 428, 261–285. doi:10.1051/0004-6361:20041335
- Leng, M. J., and Marshall, J. D. (2004). Palaeoclimate Interpretation of Stable Isotope Data from Lake Sediment Archives. *Quat. Sci. Rev.* 23, 811–831. doi:10.1016/j.quascirev.2003.06.012
- Merrill, R. T., McElhinny, M. W., and McFadden, P. L. (1996). *The Magnetic Field of the Earth Paleomagnetism, the Core, and the Deep Mantle*. San Diego: Academic Press.
- Meyers, P. A. (2003). Applications of Organic Geochemistry to Paleolimnological Reconstructions: a Summary of Examples from the Laurentian Great Lakes. *Org. Geochem.* 34, 261–289. doi:10.1016/S0146-6380(02)00168-7
- Mischke, S., Rajabov, I., Mustaeva, N., Zhang, C., Herzsich, U., Boomer, I., et al. (2010). Modern Hydrology and Late Holocene History of Lake Karakul, Eastern Pamirs (Tajikistan): A Reconnaissance Study. *Palaeogeogr. Palaeoclimatol. Palaeoecol.* 289, 10–24. doi:10.1016/j.palaeo.2010.02.004
- Mohtadi, M., Prange, M., and Steinke, S. (2016). Palaeoclimatic Insights into Forcing and Response of Monsoon Rainfall. *Nature* 533, 191–199. doi:10.1038/nature17450
- Neumann, K., Lyons, W. B., Priscu, J. C., Desmarais, D. J., and Welch, K. A. (2004). The Carbon Isotopic Composition of Dissolved Inorganic Carbon in Perennially Ice-Covered Antarctic Lakes: Searching for a Biogenic Signature. *Ann. Glaciol.* 39, 518–524. doi:10.3189/172756404781814465
- Nilsson, A., Holme, R., Korte, M., Suttie, N., and Hill, M. (2014). Reconstructing Holocene Geomagnetic Field Variation: New Methods, Models and Implications. *Geophys. J. Int.* 198, 229–248. doi:10.1093/gji/ggu120
- Nowaczyk, N. R., Liu, J., and Arz, H. W. (2020). Records of the Laschamps Geomagnetic Polarity Excursion from Black Sea Sediments: Magnetite versus Greigite, Discrete Sample versus U-Channel Data. *Geophys. J. Int.* 224, 1079–1095. doi:10.1093/gji/ggaa506
- Park, H.-S., Kim, S.-J., Stewart, A. L., Son, S.-W., and Seo, K.-H. (2019). Mid-Holocene Northern Hemisphere Warming Driven by Arctic Amplification. *Sci. Adv.* 5, eaax8203. doi:10.1126/sciadv.aax8203
- Peck, J. A., King, J. W., Colman, S. M., and Kravchinsky, V. A. (1996). An 84-kyr Paleomagnetic Record from the Sediments of Lake Baikal, Siberia. *J. Geophys. Res.* 101, 11365–11385. doi:10.1029/96JB00328
- Pilla, R. M., and Williamson, C. E. (2021). Earlier Ice Breakup Induces Change-point Responses in Duration and Variability of Spring Mixing and Summer Stratification in Dimictic Lakes. *Limnol. Oceanogr.* 67, S173–S183. doi:10.1002/lno.11888
- Prokopenko, A. A., Khursevich, G. K., Bezrukova, E. V., Kuzmin, M. I., Boes, X., Williams, D. F., et al. (2007). Paleoenvironmental Proxy Records from Lake Hovsgol, Mongolia, and a Synthesis of Holocene Climate Change in the Lake Baikal Watershed. *Quat. Res.* 68, 2–17. doi:10.1016/j.yqres.2007.03.008
- Reimer, P. J., Austin, W. E. N., Bard, E., Bayliss, A., Blackwell, P. G., Bronk Ramsey, C., et al. (2020). The IntCal20 Northern Hemisphere Radiocarbon Age Calibration Curve (0–55 Cal kBP). *Radiocarbon* 62, 725–757. doi:10.1017/RDC.2020.41

- Renssen, H., Seppä, H., Heiri, O., Roche, D. M., Goosse, H., and Fichet, T. (2009). The Spatial and Temporal Complexity of the Holocene Thermal Maximum. *Nat. Geosci.* 2, 411–414. doi:10.1038/ngeo513
- Rudaya, N., Nazarova, L., Frolova, L., Palagushkina, O., Soenov, V., Cao, X., et al. (2021). The Link between Climate Change and Biodiversity of Lacustrine Inhabitants and Terrestrial Plant Communities of the Uvs Nuur Basin (Mongolia) during the Last Three Millennia. *Holocene* 31, 095968362110190–095968362111458. doi:10.1177/09596836211019093
- Ruff, M., Fahrni, S., Gäggeler, H. W., Hajdas, I., Suter, M., Synal, H.-A., et al. (2010). On-line Radiocarbon Measurements of Small Samples Using Elemental Analyzer and MICADAS Gas Ion Source. *Radiocarbon* 52, 1645–1656. doi:10.1017/S003382220005637X
- Salazar, G., Zhang, Y. L., Agrios, K., and Szidat, S. (2015). Development of a Method for Fast and Automatic Radiocarbon Measurement of Aerosol Samples by Online Coupling of an Elemental Analyzer with a MICADAS AMS. *Nucl. Instrum. Methods Phys. Res. Sect. B Beam Interact. Mater. Atoms* 361, 163–167. doi:10.1016/j.nimb.2015.03.051
- Steinhilber, F., Beer, J., and Fröhlich, C. (2009). Total Solar Irradiance during the Holocene. *Geophys. Res. Lett.* 36 (9). doi:10.1029/2009GL040142
- Stoner, J. S., and St-Onge, G. (2007). Chapter Three Magnetic Stratigraphy in Paleooceanography: Reversals, Excursions, Paleointensity, and Secular Variation. *Proxies Late Cenozoic Paleooceanogr.* 1. 99–138. doi:10.1016/s1572-5480(07)01008-1
- Striegl, R. G., Kortelainen, P., Chanton, J. P., Wickland, K. P., Bugna, G. C., and Rantakari, M. (2001). Carbon Dioxide Partial Pressure and ^{13}C Content of North Temperate and Boreal Lakes at Spring Ice Melt. *Limnol. Oceanogr.* 46, 941–945. doi:10.4319/lo.2001.46.4.0941
- Struck, J., Bliedtner, M., Strobel, P., Taylor, W., Biskop, S., Plessen, B., et al. (2022). Central Mongolian Lake Sediments Reveal New Insights on Climate Change and Equestrian Empires in the Eastern Steppes. *Sci. Rep.* 12 (2829), S173–S183. doi:10.1038/s41598-022-06659-w
- Szidat, S., Salazar, G. A., Vogel, E., Battaglia, M., Wacker, L., Synal, H.-A., et al. (2014). ^{14}C Analysis and Sample Preparation at the New Bern Laboratory for the Analysis of Radiocarbon with AMS (LARA). *Radiocarbon* 56, 561–566. doi:10.2458/56.17457
- Tian, F., Herzsuh, U., Dallmeyer, A., Xu, Q., Mischke, S., and Biskaborn, B. K. (2013). Environmental Variability in the Monsoon-Westerlies Transition Zone during the Last 1200 years: Lake Sediment Analyses from Central Mongolia and Supra-regional Synthesis. *Quat. Sci. Rev.* 73, 31–47. doi:10.1016/j.quascirev.2013.05.005
- Unkelbach, J., Dulamsuren, C., Klinge, M., and Behling, H. (2021). Holocene High-Resolution Forest-Steppe and Environmental Dynamics in the Tarvagatai Mountains, North-Central Mongolia, over the Last 9570 Cal Yr BP. *Quat. Sci. Rev.* 266, 107076. doi:10.1016/j.quascirev.2021.107076
- Wacker, L., Bonani, G., Friedrich, M., Hajdas, I., Kromer, B., Němec, M., et al. (2010). MICADAS: Routine and High-Precision Radiocarbon Dating. *Radiocarbon* 52, 252–262. doi:10.1017/S0033822200045288
- Wang, W., Ma, Y., Feng, Z., Narantsetseg, T., Liu, K.-B., and Zhai, X. (2011). A Prolonged Dry Mid-holocene Climate Revealed by Pollen and Diatom Records from Lake Ugii Nuur in Central Mongolia. *Quat. Int.* 229, 74–83. doi:10.1016/j.quaint.2010.06.005
- Wanner, H., Beer, J., Bütikofer, J., Crowley, T. J., Cubasch, U., Flückiger, J., et al. (2008). Mid- to Late Holocene Climate Change: an Overview. *Quat. Sci. Rev.* 27, 1791–1828. doi:10.1016/j.quascirev.2008.06.013
- Weltje, G. J., and Tjallingii, R. (2008). Calibration of XRF Core Scanners for Quantitative Geochemical Logging of Sediment Cores: Theory and Application. *Earth Planet. Sci. Lett.* 274, 423–438. doi:10.1016/j.epsl.2008.07.054
- Willemse, N. W., and Törnqvist, T. E. (1999). Holocene Century-Scale Temperature Variability from West Greenland Lake Records. *Geol* 27 (7), 580–584. doi:10.1130/0091-7613(1999)027<0580:hcstvfv>2.3.co;2
- Yang, Y., Ran, M., and Sun, A. (2020). Pollen-recorded Bioclimatic Variations of the Last ~2000 Years Retrieved from Bayan Nuur in the Western Mongolian Plateau. *Boreas* 49, 350–362. doi:10.1111/bor.12423
- Zhao, J., An, C.-B., Huang, Y., Morrill, C., and Chen, F.-H. (2017). Contrasting Early Holocene Temperature Variations between Monsoonal East Asia and Westerly Dominated Central Asia. *Quat. Sci. Rev.* 178, 14–23. doi:10.1016/j.quascirev.2017.10.036
- Zhu, L., Lü, X., Wang, J., Peng, P., Kasper, T., Daut, G., et al. (2015). Climate Change on the Tibetan Plateau in Response to Shifting Atmospheric Circulation since the LGM. *Sci. Rep.* 5, 13318. doi:10.1038/srep13318

Conflict of Interest: The authors declare that the research was conducted in the absence of any commercial or financial relationships that could be construed as a potential conflict of interest.

Publisher's Note: All claims expressed in this article are solely those of the authors and do not necessarily represent those of their affiliated organizations, or those of the publisher, the editors and the reviewers. Any product that may be evaluated in this article, or claim that may be made by its manufacturer, is not guaranteed or endorsed by the publisher.

Copyright © 2022 Bliedtner, Strobel, Struck, Salazar, Szidat, Nowaczyk, Bazarradnaa, Lloren, Dubois, Habertzell and Zech. This is an open-access article distributed under the terms of the Creative Commons Attribution License (CC BY). The use, distribution or reproduction in other forums is permitted, provided the original author(s) and the copyright owner(s) are credited and that the original publication in this journal is cited, in accordance with accepted academic practice. No use, distribution or reproduction is permitted which does not comply with these terms.